

Spin Wave Dispersion on the Nanometer Scale

C. L. Gao,¹ A. Ernst,¹ G. Fischer,² W. Hergert,² P. Bruno,^{1,3} W. Wulfhekel,^{1,4} and J. Kirschner¹

¹Max-Planck-Institut für Mikrostrukturphysik, Weinberg 2, 06120 Halle, Germany

²Martin-Luther-Universität Halle-Wittenberg, Institut für Physik, 06099 Halle, Germany

³European Synchrotron Radiation Facility—BP 220 F-38043 Grenoble Cedex, France

⁴Physikalisches Institut, Universität Karlsruhe (TH), Wolfgang-Gaede Strasse 1, 76131 Karlsruhe, Germany

(Received 24 July 2008; published 13 October 2008)

Hot electrons injected into antiferromagnetic Mn layers from the tip of a low temperature scanning tunneling microscope have been used to determine the energies, lifetimes, and momenta of antiferromagnetic spin waves on the nanometer scale. The spin waves show a linear dispersion with a velocity of 160 ± 10 meV Å and lifetimes that scale linearly with energy in agreement with neutron scattering and theory. It is shown that the method is sensitive enough to detect the influence of surface anisotropies on the spin wave dispersion.

DOI: [10.1103/PhysRevLett.101.167201](https://doi.org/10.1103/PhysRevLett.101.167201)

PACS numbers: 75.30.Ds, 75.30.Gw, 75.50.Ee, 75.70.-i

Ferromagnetic and antiferromagnetic systems play important roles in modern information technology ranging from magnetic data storage to sensors or magnetic random access memory. For a functioning device, not only the ground state properties of magnetic materials are of interest. Every time the device is switched, i.e., when a field is sensed or data are written, the magnetic system is excited. The fundamental excitations of magnets are collective excitations of the magnetic moments called spin waves. Spin waves are at the heart of physical properties such as fast magnetization reversal [1], zero bias anomalies in magnetic tunneling junctions [2], or current induced magnetic switching [3–5]. While a deep understanding of spin waves on the nanometer scale is desirable for the improvement of modern spin electronic devices [6,7], established experimental techniques like Brillouin light scattering, inelastic neutron scattering (INS), or spin polarized electron energy loss spectroscopy (SPEELS) [8] lack of the sensitivity for the study of spin waves in individual nanostructures or do not offer a high lateral resolution. Recently, scanning tunneling microscopy (STM) has been used to study the energetics of spin flip scattering in magnetic films, atomic chains, and single atoms [9–11]. Here we demonstrate that beyond the lateral resolution, STM can also be used to determine the momenta and lifetimes of collective excitations such that the full dispersion relation of spin waves in nanoscopic objects can be obtained. The combination of high lateral resolution, high sensitivity, and information of momenta and lifetimes opens up a whole new field that was inaccessible so far by established scattering techniques.

This new technique is based on inelastic scanning tunneling spectroscopy (ISTS). In ISTS, the tunneling electrons inelastically interact with one of the electrodes [12]. When the tunneling electrons have enough kinetic energy (eU) to excite an inelastic process, the tunneling current is enhanced. The onset of the inelastic scattering process

creates a step in the differential conductivity dI/dU or a peak in the d^2I/dU^2 . Inelastic excitations may occur in the forward and backward tunneling direction, leading to peaks in d^2I/dU^2 with odd symmetry in U [9,12].

We here report on the local creation of spin waves with ISTS in nm thin γ -Mn films which are grown by molecular beam epitaxy on clean $\text{Cu}_3\text{Au}(001)$ crystal in ultrahigh vacuum at room temperature. In contrast to the complex bulk phase of α -Mn with 58 atoms in the unit cell, the simple face centered cubic (fcc) γ -Mn can be stabilized as ultrathin films on $\text{Cu}_3\text{Au}(001)$ [13]. The electron diffraction has revealed there is a small change of the interlayer distances from 1.87 Å (i.e., nearly fcc Mn) to 1.77 Å at a thickness around 10 atomic layers (ML) [13]. The γ -Mn films show a layerwise antiferromagnetic order [13,14]. After sample preparation, the samples were transferred to the 5 K STM, where the inelastic tunneling spectra were measured using a lock-in technique detecting the second harmonics of a 17 kHz modulation of an amplitude of 3 mV. The spectra were taken on several points of an atomic terrace and were averaged to enhance the signal-to-noise ratio.

Figure 1 shows the typical morphologies of Mn films on $\text{Cu}_3\text{Au}(001)$. At coverages below 10 ML, only two atomic layers are exposed while at higher coverages, the film roughens slightly and shows square patches of flat Mn terraces separated by multiple steps. The Mn films stay in the fcc or tetragonal (fct) structure over the whole thickness range studied [13]. The ISTS measurements were performed on the Mn films in a thickness range from 4 ML to 24 ML on individual nanometer scale Mn terraces.

In bulk magnetic materials, spin waves are free to travel in all three dimensions resulting in a continuous dispersion of the spin wave energy E with the three-dimensional momentum k . If one restricts one of the dimensions (say the z direction) going to the thin film geometry, due to the

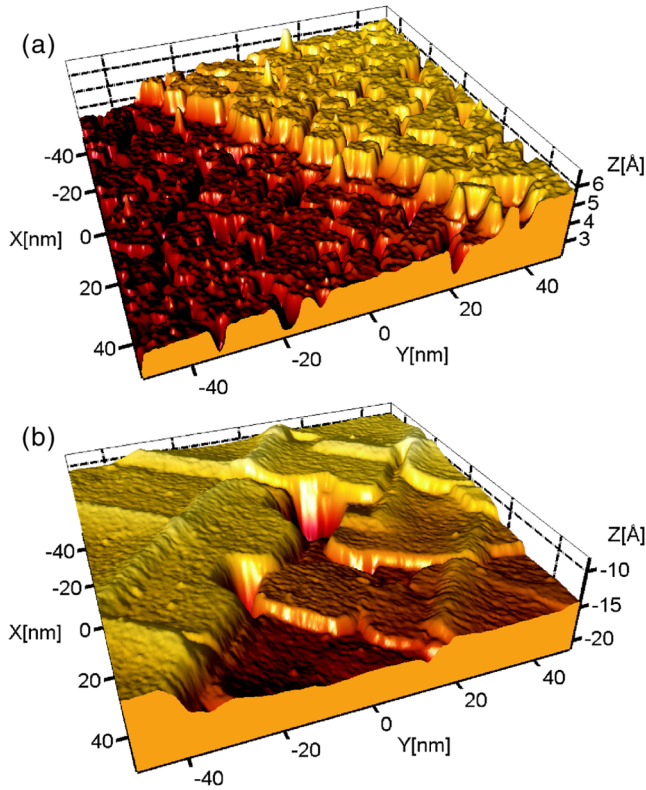


FIG. 1 (color online). Topographies of (a) 5.8 ML and (b) 24 ML Mn on $\text{Cu}_3\text{Au}(001)$.

confinement of the two boundaries (interfaces), spin waves are scattered back and forth between the boundaries. If the film thickness equals the integral multiple of the half wavelength projected along z , standing waves are formed [15]. Such standing spin waves can be regarded as oscillations of the magnetization which are nonuniform in the direction normal to the surface and which travel freely in the two other dimensions. Therefore, the dispersion relation is given by a series of spin wave branches quantized in the momentum perpendicular to the plane k_z and continuous in the momenta in the plane k_x and k_y .

The d^2I/dU^2 spectra recorded on thin films of thicknesses as indicated, are shown in Fig. 2. No variations of the inelastic spectra were observed within single terraces. This is due to their large size, i.e., small energy splitting of potentially laterally confined spin waves, and the weak confinement due to coupling to neighboring terraces. Note that the local roughness of only 10 pm is small compared to the wave length of spin waves and does not influence their energy. The peaks are antisymmetric with respect to zero bias voltage indicating an inelastic excitation by the tunneling electrons either from tip to sample (positive voltages) or vice versa (negative voltages) [12]. The antisymmetry of the excitation peaks as well as their low energy excludes quantum well states. The latter are not symmetric with respect to the Fermi level and show a much stronger dispersion. As both the Cu_3Au substrate and the

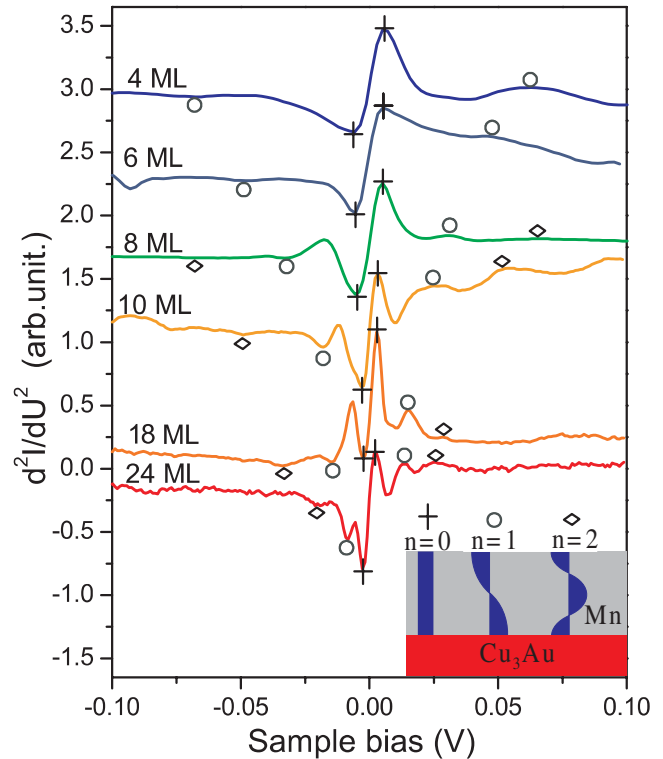


FIG. 2 (color online). d^2I/dU^2 spectra of various thicknesses Mn thin films on $\text{Cu}_3\text{Au}(001)$. The zero order (cross), first order (circle), and second order (parallelogram) excitation peaks are marked in the figure. These excitations correspond to standing spin waves as sketched in the inset.

vacuum above the antiferromagnetic film are nonmagnetic, the surface and interface spins of the antiferromagnetic layer are not pinned at the interfaces and are free to rotate. Thus, spin waves in the antiferromagnet are reflected with no phase shift at both interfaces and the standing spin waves can be classified by the order $n = 0, 1, 2$, where n reflects the number of nodes in the standing waves along z . They are sketched in the inset of Fig. 2. In agreement with this simple quantization of the spin wave momentum perpendicular to the sample plane, we observe a series of excitation peaks in the inelastic spectra, which are indicated in Fig. 2. In the experiment, only the Mn films with even atomic layers fulfill these simple quantization, while spectra from the films with odd atomic layers in principle act as ferrimagnets and lose this simple behavior. In general, the density of states of spin waves confined in z should rise in steps, as every two-dimensional branch of the spin wave spectrum adds density of states starting from its band bottom. However, the cross section for electron-electron scattering that is responsible for the creation of spin waves falls off with the in-plane spin wave momenta k_x and k_y as has been shown in SPEELS experiments [16]. This implies that the onset of every branch of standing spin waves is observed as a peak in ISTS. The zero order excitation corresponds to the energy gap at $k_x = k_y = k_z = 0$, which

is the coherent rotation of the magnetic moments of the antiferromagnet. The gap is due to the presence of the magnetic anisotropy interacting with the exchange energy as proposed by Anderson in 1952 [17]. In the spectra in Fig. 2, the zero order excitations are marked by the crosses. Besides the peak of the $n = 0$ branch, peaks of higher order can be seen in the spectra. The first order excitation has the wavelength of twice of the film thickness while the wavelength of the second order excitation equals the film thickness as shown in the inset of Fig. 2. The first and second order peaks are marked by the circle and parallelogram, respectively. As can be seen from the figure, at high coverage, the peaks are rather sharp while at low coverage, the peaks are broadened. Thus, the higher order excitations are only observable clearly at high coverage.

From the thickness t of the Mn layer and the order of the peak, we can compute the momentum k using a simple conversion $k_z = n\pi/t$. This way, both the energy E and the momentum k_z of the spin wave can be obtained from the local excitation spectra. This information characterizes the nature of the excitation and represents its discrete dispersion. Phonons can be excluded since their dispersion does not have a gap at $k = 0$ while this gap is a signature of spin waves in antiferromagnets. Figure 3 gives the resulting dispersion deep into the Brillouin zone. At low wave vector, the energy of the spin waves increases linearly as expected for antiferromagnetic spin waves. Though a structural transition from fcc to fct happens at about 10 ML during the growth, no abrupt change was present in the dispersion curve. This can be either due to the fact

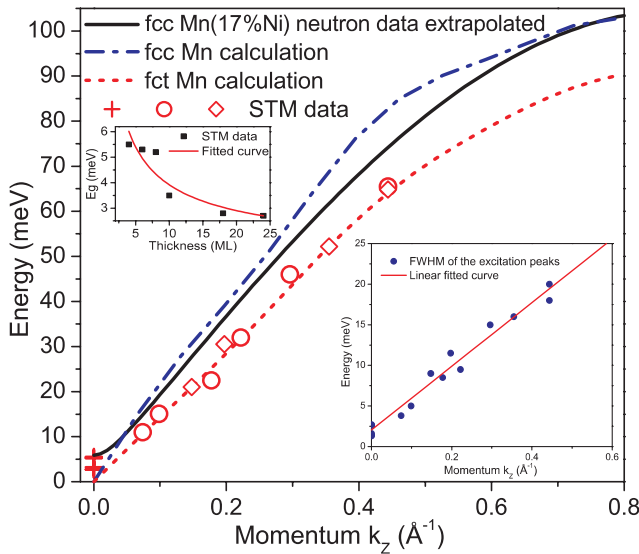


FIG. 3 (color online). Spin wave dispersion of γ -Mn. The notations (cross, circle, parallelogram) of STM data are the same as in Fig. 2. The extrapolated neutron scattering data is from [18]. The fcc and fct Mn dispersions were obtained by *ab initio* calculations. The upper inset gives the gap E_g as a function of film thickness (see text) and the lower, the FWHM as a function of k .

that the magnetic structures and spin wave dispersions of the two phases are nearly identical (see our calculations below and Ref [14]) or the room temperature fcc phase transforms to fct upon cooling as the fcc to fct transition is related to the onset of antiferromagnetism [13]. Thus, we can combine all individual energy-momentum data points to a dispersion curve and obtain the spin wave velocity of 160 ± 10 meV \AA by fitting the results with the dispersion relation $E_k^2 = E_g^2 + [v \sin(ka)/a]^2$ of antiferromagnetic spin waves, where E_k is the spin wave energy, E_g is the energy gap, a is the interlayer distance, and v is the spin wave velocity. In comparison, we plotted the extrapolated INS data of Ni doped fcc Mn [18]. The dispersion curve of Ni doped fcc Mn is slightly steeper than our STM results, but in general agrees well with our findings.

Furthermore, we can measure the full width of half maximum (FWHM) of the excitation peaks from the spectra shown in Fig. 2. These give the damping of the spin waves $\Gamma(k)$ illustrated in the lower inset of Fig. 3. As has been demonstrated in the INS experiments [18], the damping increases linearly with the wave vector (or the energy) in the first order approximation. We can use a simple linear equation $\Gamma(k) = \Gamma_0 + \Gamma_1 k$ to fit the data and gives $\Gamma_0 = 2$ meV and $\Gamma_1 = 39 \pm 2$ meV \AA . The energy broadening of the high k vector or high E excitations is related to the fact that the damping of spin waves in first order scales linearly with the precession frequency of the magnetic moments as described in the viscous damping term of the Landau-Lifshitz-Gilbert equation [19].

In order to compare our results with previous INS measurements on doped γ -Mn bulk samples, we listed the spin wave parameters together with the measurement temperature T of the reported results in Table I. These parameters depend very much on the doping and T in INS experiments. When compared to our results, we find a good agreement of the velocity. However, the damping we obtained from pure γ -Mn is smaller than doped γ -Mn. This implies that impurities in antiferromagnets are critical in determining the dynamic behavior of the system. A similar increase of damping with doping has been reported before for ferromagnets [22].

Since the experimental preparation of pure bulk fcc Mn has not been successful so far, we performed *ab initio* calculations of the spin wave dispersion of fcc bulk Mn.

TABLE I. Comparison of the gap E_g , spin wave velocity v , and the first order damping parameter Γ_1 .

Composition	E_g (meV)	v (meV \AA)	Γ_1 (meV \AA)	T (K)
Mn (17%Ni) [18]	5.90 ± 0.2	185 ± 12	85 ± 15	100
Mn (10%Cu) [20]	12	210 ± 8	118	113
Mn (10%Fe3%Cu) [21]	12 ± 0.5	290 ± 15	100 ± 30	4.2
Pure γ -Mn [this work]	2.7–5.5	160 ± 10	39 ± 2	5

The slight tetragonal distortion of the crystal structure of Mn thin films above 10 ML was taken into account. At first the electronic structure of bulk Mn was calculated self-consistently within scalar-relativistic density functional theory [23,24] in the local spin density approximation implementing the Korringa-Kohn-Rostoker [25,26] multiple scattering theory. After convergence of the ground state, the magnetic interactions of the Mn were mapped onto an effective Heisenberg Hamiltonian of the kind $H = -\frac{1}{2}\sum_{ij}J_{ij}\vec{S}_i \cdot \vec{S}_j$, where \vec{S}_i and \vec{S}_j denote the magnetic moments, located at different lattice sites, and J_{ij} is the exchange interaction between these moments. The spectrum of the Heisenberg Hamiltonian describes the magnetic excitations within the adiabatic approximation, which assumes that the characteristic time scale for the dynamics of spin fluctuations is comparable with the time scale for the dynamics of band electrons. The exchange parameters J_{ij} were computed using the magnetic force theorem [27] which describes the energy change due to a small change of the angle between the magnetic moments.

The results of the calculations for fcc and fct Mn are plotted in Fig. 3 together with the experimental results. The fct calculations perfectly fit the experimental results. As can be seen, both the experimental and theoretical energies for the high wave vector spin waves deviate from the linear dispersion. This reflects the proximity to the magnetic zone boundary. The calculated results of fcc Mn have higher energy than fct Mn at the same wave vector.

Finally, we found that the experimental energies of the $n = 0$ standing spin wave slightly increase from 2.7 to 5.5 meV as the thickness of Mn decreasing from 24 to 4 ML (see the upper inset of Fig. 3). This effect could be associated to a surface anisotropy of the antiferromagnet. As the thickness of the film decreases, the surface anisotropy becomes more and more important with respect to the bulk anisotropy influencing the spin wave gap at $k = 0$. The spin wave energy at $k = 0$ is given by $E_g = \sqrt{2E_A E_E + E_A^2}$, where E_A is the anisotropy energy and E_E is the exchange energy [28]. E_A contains the bulk anisotropy (E_{AB}) and surface anisotropy (E_{AS}): $E_A = E_{AB} + E_{AS}/t$ assuming a combined surface and interface anisotropy energy of both interfaces. Here, t is the film thickness. With the exchange energy of $E_E = 25$ meV taken from our *ab initio* calculation, we fitted E_g as a function of the film thickness (see the upper inset of Fig. 3) obtaining a small or vanishing bulk anisotropy energy of $E_{AB} = 0.02 \pm 0.03$ meV and surface anisotropy energy of $E_{AS} = 1.4 \pm 0.2$ meV per atom. These values are reasonable and in the energy range of anisotropies found in ferromagnetic structures. The bulk anisotropy energy is small such that the surface anisotropy becomes dominant in the low thickness range. In our *ab initio* calculations spin orbit coupling was not taken into account such that the gap is not present.

In summary, we have demonstrated that ISTS is capable of detecting both the energy and the momentum of standing spin waves on the nanoscale. We have determined the spin wave dispersion of antiferromagnetic fct/fcc Mn. It agrees well with *ab initio* calculations and with published INS data on doped bulk fcc Mn. The broadening of the excitations with energy shows a linear dependence in agreement with INS, but the lifetimes are significantly longer than those observed in doped Mn. This is explained by the stronger damping in doped Mn due to the dopant atoms. Finally, it is shown that the sensitivity of the technique is sufficient to detect the influence of surface anisotropies on the dispersion. As deduced from the spin wave gap of Mn films of various thicknesses, a surface or interface anisotropy of the order of 1.4 meV per atom was deduced. This new technique offers a unique sensitivity and lateral resolution such that the determination of the magnetic excitation spectra of nanoscopic ferromagnetic or antiferromagnetic structures comes within reach.

-
- [1] I. Tudosa *et al.*, Nature (London) **428**, 831 (2004).
 - [2] J. S. Moodera, J. Nowak, and R. J. M. van de Veerdonk, Phys. Rev. Lett. **80**, 2941 (1998).
 - [3] G. D. Fuchs *et al.*, Appl. Phys. Lett. **85**, 1205 (2004).
 - [4] J. C. Sankey *et al.*, Nature Phys. **4**, 67 (2008).
 - [5] H. Kubota *et al.*, Nature Phys. **4**, 37 (2008).
 - [6] G. A. Prinz, Science **282**, 1660 (1998).
 - [7] S. A. Wolf *et al.*, Science **294**, 1488 (2001).
 - [8] R. Vollmer *et al.*, Phys. Rev. Lett. **91**, 147201 (2003).
 - [9] C. F. Hirjibehedin *et al.*, Science **317**, 1199 (2007).
 - [10] C. F. Hirjibehedin, C. P. Lutz, and A. J. Heinrich, Science **312**, 1021 (2006).
 - [11] T. Balashov *et al.*, Phys. Rev. Lett. **97**, 187201 (2006).
 - [12] E. L. Wolf, *Principles of Electron Tunneling Spectroscopy* (Oxford University Press, New York, 1985).
 - [13] W. C. Lin *et al.*, Phys. Rev. B **75**, 054419 (2007).
 - [14] J. Hafner and D. Spišák, Phys. Rev. B **72**, 144420 (2005).
 - [15] C. Kittel, Phys. Rev. **110**, 1295 (1958).
 - [16] W. X. Tang *et al.*, Phys. Rev. Lett. **99**, 087202 (2007).
 - [17] P. W. Anderson, Phys. Rev. **86**, 694 (1952).
 - [18] J. Jankowska-Kisielińska, K. Mikke, and J. J. Milczarek, J. Magn. Magn. Mater. **140-144**, 1973 (1995).
 - [19] A. Aharoni, *Introduction to the Theory of Ferromagnetism* (Oxford University Press, New York, 2001).
 - [20] J. A. Fernandez-Baca *et al.*, J. Appl. Phys. **73**, 6548 (1993).
 - [21] K. Mikke, J. Jankowska, and E. Jaworska, Physica (Amsterdam) **120B+C**, 156 (1983).
 - [22] J. O. Rantschler *et al.*, J. Appl. Phys. **101**, 033911 (2007).
 - [23] W. Kohn and L. J. Sham, Phys. Rev. **140**, A1133 (1965).
 - [24] P. Hohenberg and W. Kohn, Phys. Rev. **136**, B864 (1964).
 - [25] J. Korringa, Physica (Amsterdam) **13**, 392 (1947).
 - [26] W. Kohn and N. Rostoker, Phys. Rev. **94**, 1111 (1954).
 - [27] A. I. Liechtenstein *et al.*, J. Magn. Magn. Mater. **67**, 65 (1987).
 - [28] *Ferromagnetismus*, edited by H. P. J. Wijn, Handbuch der Physik Band XVIII/2 (Springer-Verlag, Berlin, 1966).